JADE family proteins regulate proteasome abundance and activity

Lena Kathrin Ebert[1], Sebastian Bargfrede[1], Katrin Bohl[1], Roman-Ulrich Müller[1,2], Thomas Benzing[1,2], Bernhard Schermer[1,2,#]

[1] *Department II of Internal Medicine and Center for Molecular Medicine Cologne, University of Cologne, Faculty of Medicine and University Hospital Cologne, Cologne, Germany.*

[2] *CECAD, University of Cologne, Faculty of Medicine and University Hospital Cologne, Cologne, Germany.*

[#] *corresponding author*

Email: bernhard.schermer@uk-koeln.de

Running title: Jade proteins control proteasomal activity

Key words: PHD finger, kidney, proteasome, ubiquitination, primary cilium

Abstract

JADE family proteins (JADE1/2/3) have been implicated in diverse cellular functions and signaling pathways ranging from WNT signaling and cell cycle control to cell death and complex transcriptional regulation through histone acetyl-transferase complexes. JADE proteins show a high degree of sequence similarity and share two PHD zinc finger domains. JADE1 interacts with cilia-associated proteins and has been implicated in cilia-related genetic disorders with kidney phenotypes. However, the function of the widely expressed JADE proteins at the molecular level is still elusive. Here we show that JADE proteins regulate proteasome abundance and activity. Using kidney cells as a model, we demonstrate that loss of either JADE protein resulted in increased expression of almost all components of the 26S proteasome. Regulation occurred at the post-translational level and was not the consequence of transcriptional activation. Consistent with a role for JADE proteins in regulating overall proteasomal abundance, proteasomal activity was elevated in Jade-deficient cells, while exogenous expression of JADE1/2/3 decreased the level of proteasome activity. Coimmunoprecipitation experiments confirmed the interaction of proteasomal subunits with Jade1 suggesting a direct role of JADE proteins in regulating turnover, stability and abundance of the 26s proteasome. These data may now explain the plethora of cellular roles that have been attributed to JADE proteins.

Introduction

The plant-homeodomain (PHD) zinc finger protein JADE1 (PHF17; Gene for Apoptosis and Differentiation in Epithelia 1) has been initially identified as interactor of the tumor suppressor pVHL in a yeast two-hybrid screen (1). Mutations in *VHL* cause the autosomal-dominant von-Hippel Lindau (VHL) disease, a hereditary tumor syndrome associated with hemangioblastomas, pheochromocytomas and clear-cell renal cell carcinoma (ccRCC). Aberrations of *VHL* are also found in the majority of sporadic ccRCCs (2–5). It has been shown that JADE1 is stabilized by pVHL and this stabilization is diminished if *VHL* carries pathogenic mutations (1, 6–8). Moreover, JADE1 has been described as a single unit E3 ubiquitin ligase targeting beta-catenin for degradation and thereby inhibiting canonical WNT signaling (9). Both high levels of β-catenin and low levels of JADE1 are related to poor prognosis in RCC patients (6). This supports the current notion of JADE1 as a putative tumor suppressor in the kidney, related to pVHL. In addition, JADE1 forms a protein complex with members of the NPHP protein family, in particular NPHP4. Mutation in the *NPHP* genes result in Nephronophthisis, an autosomal-recessive cystic kidney disease leading to kidney failure in children and adolescents (10). Similar to pVHL, NPHP4 stabilizes JADE1 and enhances inhibition of canonical WNT signaling (11). Similarly, JADE1 has been functionally linked to polycystin-1 (PC1) (12). PC1 is encoded by the *PKD1* gene, mutations of which cause autosomal-dominant polycystic kidney disease (ADPKD), the most frequent cystic kidney disease in adults. PC1, NPHP proteins and pVHL are localized to primary cilia and disorders caused by mutation of these proteins are considered ciliopathies (13). Interestingly, JADE1 has been shown to co-localize with NPHP proteins at the ciliary base (11).

Besides the connection to ciliopathy proteins and WNT signaling, JADE1 has been described as a co-factor for two histone acetyltransferases (HATs), HBO1 and its homologue Tip60, thereby inducing histone H4 acetylation (14, 15). This implicates functions of JADE1 that affect transcriptional and epigenetic regulations, DNA metabolism, as well as cell cycle regulation (14, 16, 17). Surprisingly, a gene trap mouse model targeting *Jade1* did not develop any major phenotype (18). This led to the hypothesis that additional proteins could functionally overlap and compensate for the loss of JADE1. Obviously, the additional members of the Jade protein family, JADE2 (PHF15) and JADE3 (PHF16), are key candidates for this compensation (18). The *JADE* genes, encoding for the three individual JADE proteins, are located on three different chromosomes (chr. 4, chr. 5, chr. X in the human genome and chr. 3, chr. 11 and chr. X in the mouse genome). As we will demonstrate in detail, all three JADE proteins share a high percentage of sequence similarity and conserved protein domains (19). Little is known about specific functions of JADE2 and JADE3, but a few studies provide some evidence for similar pathways and functions within the JADE family: Similar to JADE1, JADE2 was suggested to act as an E3-ubiquitin ligase that targets the histone H3K4 demethylase LSD1 (20–22) and JADE3 has been

65 found to be induced by WNT/β-catenin and to have oncogenic properties in colon cancer (23).
66 Moreover, all three JADE proteins are part of the HBO1 complex (14, 17, 24).
67 While JADE family members have been implicated with a variety of different pathways and processes,
68 their molecular function has never been directly compared in the same tissue or cell type. Here, we
69 analyzed common and individual functions of *Jade1*, *Jade2*, and *Jade3* in differentiated murine renal
70 tubular epithelial cells. Using CRISPR/Cas9-mediated genome editing, we generated monoclonal loss-
71 of-function cell lines with two independent strategies for each of the *Jade* genes, which resulted in two
72 deficient cell lines per *Jade* gene. After demonstrating the lack of Jade expression and the absence of
73 any counter-regulation on mRNA and protein level, we performed unbiased proteomic, transcriptomic
74 and in-depth bioinformatic analyses to understand the individual alterations upon loss of Jade1, Jade2
75 and Jade3. Taken together, we identified and confirmed increased proteasomal abundance and activity
76 as a common molecular phenotype of JADE-deficient cells.
77
78 **Results**
79 *JADE protein family members share common interactors related to renal disease.*
80 JADE proteins share two PHD zinc finger domains, several PEST domains, and nuclear localization
81 signals (Fig. 1A). Based on their structural similarities, we sought to investigate whether JADE2 and
82 JADE3 share molecular functions with JADE1. JADE1 has been characterized as an interactor of the
83 ciliary protein pVHL (7) and of the nephrocystin protein complex (11). Therefore, we cloned the cDNA
84 of human JADE2 and JADE3 in expression vectors and performed coimmunoprecipitation experiments,
85 which included JADE1S as positive control. V5-tagged pVHL (V5.VHL) was co-expressed together with
86 JADE1S (F.Jade1S), JADE2, JADE3, or a control protein, all with an N-terminal Flag-tagged. These
87 experiments revealed pVHL to co-precipitate with all three JADE proteins (Fig. 1B). We performed
88 similar experiments with V5.NPHP4 (Fig. 1C) and V5.NPHP1 (Fig. 1D). Again, both NPHP4 and NPHP1
89 specifically co-precipitated with all of the JADE proteins. Additional co-immunoprecipitation
90 experiments with differently-tagged JADE proteins supported the idea, that JADE proteins form
91 homodimers or homomultimers (Fig. 1E,F). Given the high structural similarity between the individual
92 JADE proteins we assumed that JADE1/2/3 could also built hetero-multimeric protein complexes. This
93 notion was confirmed by coimmunoprecipitation among the different JADE proteins (Fig. 1G). In
94 summary, all JADE proteins share relevant renal protein complexes, very similar to their putative
95 common role as co-factors and components of the HBO1/HAT complex (14, 24), indicating that they
96 could interact in the same complex with a common function.
97
98
99

100 *JADE family members show ubiquitous transcription with spikes in different tissues.*
101 The N-terminal part of the JADE proteins shows the highest level of similarity as illustrated by the
102 higher protein identity score between JADE2/3 and JADE1S compared to JADE1L (Supplemental Fig.
103 S1A) (19). We used available data sets of the Human Protein Atlas to analyze tissue expression. Protein
104 expression data was only available for JADE1 and shows global expression in most tissues with
105 squamous epithelial cells of the oral mucosa, esophagus, and uterine, as well as hepatocytes and
106 kidney tubules expressing the highest levels (Supplemental Fig. S1B). mRNA expression data support
107 the ubiquitous expression of *JADE1* in most tissues with higher levels in the pancreas and endocrine
108 and female tissues (Fig. S1C). *JADE2* appears ubiquitously expressed in most tissues with enrichment
109 in the brain, endocrine tissues, female tissues, and lymphoid tissue. The overall *JADE3* expression is
110 relatively low as compared to *JADE1* and *JADE2*. The expression pattern is similar to *JADE2* with the
111 highest levels in the brain, endocrine tissues, female and male tissues, and lymphoid tissues
112 (Supplemental Fig. S1C). Importantly, while the expression of all three JADE genes is confirmed in most
113 tissues, there is generally one JADE family member predominantly expressed (e.g., JADE1 in pancreas,
114 bone marrow, or breast; JADE2 in cerebral cortex, lymph nodes, and midbrain; JADE3 in epididymis,
115 placenta, and testis). In addition, the *JADE* family is conserved across species and has a target identity
116 matching the mouse orthologue to the human sequences of 92.45 %, 91.44 %, and 81.92 %, for JADE1,
117 JADE2, and JADE3, respectively (25). Single-cell transcriptomic data from mouse kidneys revealed that
118 all Jade proteins are expressed in the kidney with a predominance of *Jade1* over *Jade2* and *Jade3* and
119 with co-expression of all three proteins in cells of the collecting duct (Supplemental Fig. S1D) (26).
120 Therefore, we decided to target Jade expression in this specific cell type.
121
122 *Loss-of-function mutations in one Jade gene reveals independent expression of the remaining family*
123 *members.*
124 To analyze and compare transcriptional and translational consequences of Jade protein deficiency, we
125 used the established mIMCD3 (murine inner medulla collecting duct 3) cell line and targeted individual
126 *Jade* genes with CRISPR/Cas9. We designed two individual non-overlapping sgRNAs (single-guide RNAs)
127 for each of the *Jade* genes to account for potential off-target effects. The first sgRNA was targeted to
128 the region encoding the first PHD domain, the second sgRNA to the downstream exon containing the
129 second PHD domain's start (Supplemental Fig. S2A). Mutant monoclonal cell lines were screened and
130 validated by PCR and Sanger sequencing; the resulting mutant Jade protein structures are depicted in
131 Supplemental Fig. S2B. When performing qPCR analyses for the different *Jade* genes, we observed a
132 significant reduction of mRNA expression of the targeted Jade gene in the respective mutant cell line
133 (Fig. 2A-C). Targeted proteomic PRM assays confirmed the absence of individual Jade protein

134 expression in the specific Jade-deficient cell lines (Fig. 2D-F). Remarkably, we do not observe any
135 compensatory upregulation of the remaining Jade family members on transcript and protein level.
136
137 *Proteomic analyses of Jade deficient cell lines reveal an increased abundance of almost all*
138 *proteasomal components.*
139 We next performed unbiased proteomic analysis from all six Jade-deficient cell lines and the wildtype
140 control. For each Jade-deficient cell line the principal component analysis showed the clustering of the
141 replicates and the separation of WT versus the pair of mutant cell lines by the first principal component
142 (Fig. 3A-C). When plotting the Student's T-test difference of KO1 versus KO2 for each of the Jade family
143 members we found that they correlate and that expression of most deregulated proteins is shifted in
144 the same direction within both mutant cell lines for each Jade protein (Supplemental Fig. S3A-C).
145 Taking the sum of the significantly regulated proteins for both mutant cells for each Jade protein, we
146 then calculated the overlap of significantly regulated proteins between the members of the Jade
147 protein family (Fig. 3D). This revealed 644 proteins with significantly altered expression in all
148 Jade1/2/3-deficient cell lines, supporting the concept that Jade protein family members share
149 biological functions. A Gene Ontology and KEGG pathway analysis of these 644 proteins revealed terms
150 related to the 26S proteasome, ribosomes, and protein translation to be enriched (Fig. 3E). Indeed,
151 many proteins related to the proteasome were significantly upregulated in the cell lines, as shown in
152 a representative volcano blot of the Jade1 KO2 cell line (Fig. 3F) and in a heat-map summarizing the
153 results from all cell lines (Fig. 3G). We also observed an altered expression of ribosomal proteins, tRNA
154 ligases, as well as translation initiation and elongation factors in a similar manner (Supplemental Fig.
155 S3D-F), being suggestive of a high protein turnover.
156
157 *Elevated proteasomal activity in Jade deficiency.*
158 To investigate whether these changes in protein expression caused a higher proteasomal activity, we
159 monitored the degradation of a fluorogenic substrate for the chymotrypsin-like activity of the
160 proteasome. Indeed, all Jade-deficient cell lines showed a significant increase in proteasomal activity
161 as compared to the wildtype cells (Fig. 4 A). Consistently, using exogenously expressed Jade proteins,
162 we could show that the proteasome activity is reduced compared to an overexpressed control protein
163 (Fig. 4B).
164
165 *Increased proteasome abundance is not caused by transcriptional regulation.*
166 Based on the role of *Jade1/2/3* as transcriptional and putative epigenetic regulators, we aimed to
167 investigate whether the increased proteasome activity was caused by transcriptional upregulation of
168 its components. To answer this question, we performed unbiased transcriptomic analyses with mRNA-

169 Seq from all six Jade-deficient cell lines and the control cell line. For *Jade1* deficient cell lines, principal
170 component analysis showed a narrow clustering of the replicates and a clear separation of WT versus
171 mutant cell lines accounting for 75 % of the variance (Supplemental Fig. S4A). For *Jade2* and *Jade3* the
172 replicates clustered clearly together, the separation from the WT cell lines was based primarily on the
173 second principal component (Supplemental Fig. S4B,C). When plotting the fold change for KO1 versus
174 KO2 for *Jade1* we saw a clear correlation (Supplemental Fig. S4D). The same visualization for *Jade2* and
175 *Jade3* revealed that the individual mutant cell lines for each of them are less correlated than seen for
176 *Jade1* (Supplemental Fig. S4E,F). Taking the sum of the significantly regulated genes for each *Jade*
177 family member, we found that 567 genes were commonly regulated within the family (Supplemental
178 Fig. S5A). However, when we individually checked the expression of the proteasomal components
179 across all cell lines we did not observe any expression changes (Supplemental Fig. S5B,C). Additionally,
180 we did not observe an upregulation in ribosomal genes and genes encoding for tRNA ligases or
181 transcription initiation and elongation factors (Supplemental Fig. S5D-F). Taken together, the increased
182 abundance and activity of the proteasome was not based on increased transcription in the Jade
183 deficient cells.
184
185 *Proteasomal core components co-precipitate with Jade1L and Jade1S.*
186 Searching for a direct connection between the 26S proteasome and Jade proteins, we re-expressed
187 either Flag-tagged Jade1S or Jade1L or a control protein in a Jade1-deficient cell line and performed an
188 anti-Flag coimmunoprecipitation experiment. Pulled-down protein complexes were analyzed by nLC-
189 MS/MS. The heatmap of iBAQs of the proteins that are exclusively found in the Jade1L/S samples
190 shows Jade1 as most abundant among these proteins (Fig. 5A). Plotting the Student's T-test Difference
191 between Jade1L and the control versus the –log Student's T-test p-value, we observed not only several
192 known Jade1 interactors (green) but also several components of the proteasome (magenta)
193 significantly enriched in the Jade1L sample (Fig. 5B). Moreover, we could confirm the same for Jade1S.
194 Here, specifically Psma1 was among the most enriched proteins (Fig 5C).
195
196 **Discussion**
197 JADE1 and in parts the other members of the JADE protein family have been previously described as
198 components of several protein complexes and their potential cell biological functions have been mainly
199 deduced by JADE interacting or associated proteins. Based on this, JADE proteins were found to be
200 part of the HBO1/HAT complex (14), to regulate pVHL, beta-catenin and by that canonical WNT
201 signaling on multiple levels (7, 9)(11), or to be involved in cell cycle regulation through a Plk1/CK1
202 kinase module(27, 28). In addition, altered expression of JADE proteins has been identified in several
203 tumor entities, in line with their protein-protein interactions with several tumor suppressors, including

204 pVHL and Ing4 (6, 24). Up to now, research on Jade proteins was primarily focused on the short isoform
205 of JADE1 (JADE1S) (19) and not a single study has compared all three individual JADE proteins in the
206 very same cellular context. In this study, we present for the first time an unbiased comparison of the
207 proteomic and transcriptomic changes in Jade1, Jade2, and Jade3 deficient cell lines. Multiple previous
208 studies suggested a specific role of JADE1 in renal ciliopathies (VHL, NPH (6, 7, 11)), ADPKD (12), renal
209 cell carcinoma (6, 29, 30) and kidney regeneration after injury (31). Strikingly, we could confirm some
210 of the key protein-protein interactions (pVHL, NPHP1 and NPHP4) related to renal ciliopathies for all
211 three Jade proteins (Fig. 1). Therefore, we continued our work with the well-characterized renal
212 tubular epithelial cell line (mIMCD3; murine inner medullary collecting duct 3) to generate the Jade
213 deficient cell lines for the at hand comparative study. Importantly, previously published datasets
214 confirmed that renal epithelial cells of the collecting duct express all Jade proteins *in vivo*
215 (Supplemental Fig. S1D).
216 With CRISPR/Cas9 mediated genome editing, we generated two independent Jade deficient cell lines
217 for each Jade family member. These cell lines were validated by Sanger sequencing, qPCR analyses of
218 mRNA expression, and a targeted proteomics approach (Fig. 2). Proteomic expression profiling
219 revealed upregulated expression of more than 80% of the individual subunits of the 26S proteasome
220 (Fig. 3G) and we could demonstrate increased proteasome activity accordingly, underlining the
221 functional relevance of the altered proteasome abundance. This suggests that JADE proteins have a
222 common function in balancing or tuning proteasome abundance. Since this is not caused by
223 transcriptional regulation of proteasome expression as reflected by our RNASeq analyses
224 (Supplemental Fig. S4), we conclude, that Jade proteins might either modulate posttranslational
225 modifications of individual proteasome components or, unspecifically, induce the process of
226 proteophagy. At this point, the finding of proteasomal subunits co-precipitating with Jade1S and
227 Jade1L strongly suggests a direct involvement of Jade proteins in the targeting of the proteasome for
228 degradation. While the detailed underlying mechanism of this regulation still needs to be discovered,
229 the observed high proteasomal activity in Jade deficient cells has several implications in the context of
230 renal diseases. Enhanced proteasomal activity might increase the sensitivity of cells towards
231 therapeutic inhibition of the proteasome. In Jade deficient cells, proteasome inhibition might more
232 efficiently increase the unfolded protein burden and proteotoxic stress to toxic levels ultimately
233 leading to apoptotic cell death. This could be relevant both for cancer cells with low or no Jade
234 expression as well as in renal ciliopathies. Here, the disease genes pVHL, NPHP's and Polycystin-1 have
235 been demonstrated to stabilize JADE1 expression (1, 12) with mutant proteins lacking this specific
236 effect (7, 12). In consequence, the low levels of JADE in mutant cells could cause increased proteasomal
237 activity. Remarkably, the use of the proteasome inhibitor Carfilzomib has been shown to ameliorate
238 the cystic kidney phenotype in a mouse model of ADPLD (32) by increasing cell death and decreasing

239 proliferation of renal epithelial cells. In this model, Jade deregulation and the general high proteasomal
240 activity might be one of the mechanisms targeted by Carfilzomib. Proteasome inhibitors have also been
241 very recently identified among other drugs in a study screening about 8000 compounds for their effect
242 on viability of PKD deficient cells (33). Further preclinical studies in mouse models are required to
243 investigate under which exact conditions targeting the proteasome in cystic kidney could be a useful
244 option.
245 Jade1 is a protein localized at the ciliary transition zone and interacting with ciliopathy proteins,
246 suggesting that the high abundance and activity of the proteasome might affect primary cilia. In all
247 Jade deficient cell lines, we do not observe any significant change in the number of ciliated cells (data
248 not shown). The UPS however, has been shown to be essential for the regulation of primary cilia.
249 Inhibition of the proteasome with MG132 or depletion of proteasomal subunits with RNAi affects both
250 ciliogenesis and ciliary disassembly (34). Interestingly, many proteasomal subunits have been
251 identified as part of a protein complexes pulled-down with transitions zone and basal body proteins
252 NPHP2, NPHP5 and NPHP8 (35) and with BBS proteins (36). Increased global proteasomal activity has
253 not been directly linked to any ciliary function. One could speculate, that increased proteasomal
254 activity as a result of reduced JADE expression might positively affect primary cilia in renal ciliopathies.
255 Interestingly, loss of cilia has been found to suppress cyst growth in ADPKD (37). As such, loss of cilia
256 may indeed be positive in some renal ciliopathies and might be counteracted under certain conditions
257 through depletion of Jade and subsequent upregulation of proteasomal activity.
258
259 **Acknowledgements**
260 We thank Stefanie Keller and Martyna Brütting for excellent technical assistance and members of the
261 laboratories for helpful discussions. In particular, we want to thank David Vilchez for his critical advice.
262 We acknowledge the help of the CECAD proteomics core facility and the Cologne Center for Genomics,
263 Cologne, Germany. We thank the FACS & IMAGING Core Facility at Max Planck Institute for Biology of
264 Ageing, Cologne, for assisting with sorting cells for generation of Jade KO cell lines. This study was
265 supported by the German Research Foundation (SCHE1562/8-1 to BS). Roman-Ulrich Müller received
266 support from the Ministry of Science North Rhine-Westphalia (Nachwuchsgruppen.NRW 2015-2021).
267
268 **Materials and Methods**
269 *Plasmids and antibodies*
270 Plasmids containing JADE1S, pVHL, and EPS^{1-225} cDNA were previously described (11, 38). JADE1L,
271 JADE2 and JADE3 cDNA were obtained by PCR from HEK293T cDNA. Jade1S, Jade1L, Jade2, and Jade3
272 cDNA were obtained by PCR from mIMCD3 cDNA. cDNA fragments were inserted into a modified
273 pcDNA6 vector (Invitrogen) containing an N-terminal FLAG-tag using standard cloning techniques. For

274 the generation of the CRISPR/Cas9-mediated mutant cell lines the selected single guide (sg)RNAs were
275 cloned into pSpCas9(BB)-2A-GFP (PX458), gifted from Feng Zhang (Addgene plasmid #48138)(39). All
276 plasmids were verified by Sanger sequencing.
277 Primary antibodies were obtained from Sigma-Aldrich (monoclonal mouse anti-FLAG (M2), F3165,
278 1:10000; polyclonal rabbit anti-FLAG, F7425, 1:2000) and Serotec (monoclonal mouse anti-V5,
279 MCA1360, 1:5000). Secondary antibodies were obtained from Jackson ImmunoResearch (goat anti-
280 rabbit HRP-coupled, 111-035-003; goat anti-mouse HRP-coupled, 115-035-003; both 1:30000).
281
282 *Cell culture and transfections*
283 Murine inner-medullary collecting duct (mIMCD3, ATCC CRL-2123) cells were cultured in DMEM-F12
284 (Sigma-Aldrich) supplemented with 10% fetal bovine serum (FBS) and 2 mM GlutaMAX (Gibco). For
285 FACS sorted cell lines the medium was additionally supplemented with 100 U/ml Penicillin-
286 Streptomycin (Gibco). mIMCD3 subclone 8 (sc.#8) was selected after FACS sorting the parental line
287 into single cells for a higher genetic homogeneity. For the generation of the CRISPR/Cas9-mediated
288 mIMCD3 sc.#8 mutant cell lines, the cells were seeded in 6-well plates, grown to 50 % confluency and
289 transfected with Lipofectamine 2000 (Invitrogen) according to the manufacturer's instructions.
290 HEK293T cells were cultured in DMEM (Gibco) supplemented with 10% FBS. For transfection
291 experiments in HEK293T cells, the cells were seeded in 10 cm dishes and grown to 50-60% confluency.
292 Plasmid DNA was transiently transfected using the calcium phosphate method. 24 h after transfection
293 cells were harvested in 8 ml of cold PBS, centrifuged and the cell pellet was used for lysis and
294 subsequent coimmunoprecipitation. All cells were cultured at 37°C in the presence of 5% CO_2 and
295 tested negative for mycoplasmas.
296
297 *Coimmunoprecipitation*
298 HEK293T cell pellets were resuspended in 1 ml of lysis buffer (20 mM Tris (pH 7.5), 1% (v/v) TritonX-
299 100, 50 mM NaCl, 15 mM $Na_4P_2O_7$, 50 mM NaF) and incubated for 15 min at 4 °C. After homogenization
300 the cell suspension was centrifuged (20,000 x g, 15 min, 4 °C) and then the supernatant was
301 ultracentrifuged (100,000 x g, 30 min, 4 °C). 50 µl of the supernatant after ultracentrifugation was used
302 as lysate (input) and boiled with 2x Laemmli buffer. Anti-FLAG agarose beads (M2, Sigma) were added
303 to the remaining supernatant. After incubation for 1 h at 4 °C the beads were extensively washed with
304 lysis buffer and boiled in Laemmli buffer. Proteins were resolved by 10% SDS-Page (NPHP1 and NPHP4
305 coimmunoprecipitations) and 12% SDS-Page (pVHL coimmunoprecipitations).
306
307
308

309 *Generation of mutant cell lines*

310 For each member of the Jade family two sgRNAs were designed using the CRISPR finder tool
311 (http://www.sanger.ac.uk/htgt/wge/)(40) and benchling (http://benchling.com). The sgRNA
312 sequences are shown in supplemental table S1. Cloning of the sgRNA containing plasmids and
313 transfection are described above. 48 h after transfection GFP-positive cells were sorted in 96-well
314 plates on a BD FACSAriatnm III. After expanding the colonies arising from single cells, a first screening
315 for mutants was performed using PCR, followed by Sanger sequencing. Primer sequences can be
316 obtained from supplemental table S1. Validation was done by qPCR and a PRM assay.

317

318 *qPCR*

319 mIMCD3 wild type and Jade mutant cells were washed with PBS and RNA extraction was performed
320 with the Direct-zol RNA Miniprep kit (Zymo Research) following the manufacturer's instructions
321 including a DNase1 treatment step. This was followed by reverse transcription using the High-Capacity
322 cDNA Reverse Transcription kit (Applied Biosystems). Jade1/2/3 mRNA was assessed by SYBR Green
323 (Thermo Fisher Scientific) qPCR using Hprt1 as endogenous control. Primers are listed in supplemental
324 table S1. The qPCR experiments were performed on a QuantStudio 12K Flex Real_time PCR System
325 (Thermo Fisher Scientific). Data were analyzed using a student's t-test and are presented as mean +/−
326 standard error of the mean (SEM). Significance levels are indicated in the figure legends.

327

328 *PRM assays*

329 Jade protein expression has been difficult to detect by shotgun proteomics experiments. Therefore,
330 we decided to use a parallel reaction monitoring (PRM) assay (41). Preparation of the samples for
331 targeted mass spectrometry was performed as previously described (42). All samples were measured
332 by the proteomics facility at CECAD. All samples were analyzed on an Orbitrap Exploris 480 mass
333 spectrometer coupled to an EASY nLC 1200 UPLC (both Thermo Scientific). Peptides were loaded with
334 solvent A (0.1% formic acid in water) onto an in-house packed analytical column (30 cm × 75 µm I.D.,
335 filled with 2.7 µm Poroshell EC120 C18 (Agilent)). Peptides were chromatographically separated at a
336 constant flow rate of 300 nl min^{-1} using with the following gradient: initial 4 % solvent B (0.1% formic
337 acid in 80% acetonitrile), ramp to 25% B within 72 min, to 55% B within 8 min and to 95% B within 2
338 min, followed by washing and column equilibration. The Exploris was equipped with a FAIMS Pro
339 Interface (Thermo) set to a CV of -47 and operated in scheduled PRM mode. The MS1 survey scan was
340 acquired from 400 to 1000 m/z at a resolution of 120,000. Target masses were isolated in a 2 h window
341 and fragmented by HCD with collision energy of 30%. The AGC target was set to 100 % and resulting
342 spectra recorded with a resolution of 120,000. Product ions were detected in the Orbitrap at a
343 resolution of 17,500.

344 Target list generation and follow-up analysis were performed in Skyline 20.2. Unique target peptides
345 and their retention times were chosen based on their detectability in data-independent trials using the
346 identical setup and gradient. Results were compared against their theoretical spectra simulated by the
347 Prosit algorithm (43) plugin in Skyline (44, 45). Only areas with a dotp value above 0.7 were included
348 in the analysis to ensure the confidence of the result. The targets are listed in supplemental table S2.
349
350 Proteome analyses
351 For each replicate, a 10 cm dish of mIMCD3 cells of the indicated genotype was harvested and snap-
352 frozen. Pellets were resuspended in Urea buffer (8 m Urea, 50 mm ammoniumbicarbonate, Halts
353 Protease-phosphatase-inhibitor (Thermo Scientific)). After clearing of the sample (16000g, 30 min at
354 4°C) the lysates were reduced (10 mM Dithiothreitol, 1 h, RT) and alkylated (50 mM Chloroacetamide,
355 30 min, RT, in the dark). An equal amount of protein was diluted to reach a concentration of 2M urea
356 and subjected to tryptic digestion (enzyme:substrate ratio of 1:50). On the next day, double-layered
357 stage-tip clean up (C18) was performed.
358 All samples were analyzed on a Q Exactive Plus Orbitrap (Thermo Scientific) mass spectrometer that
359 was coupled to an EASY nLC (Thermo Scientific). Peptides were loaded with solvent A (0.1% formic acid
360 in water) onto an in-house packed analytical column (50 cm — 75 µm I.D., filled with 2.7 µm Poroshell
361 EC120 C18, Agilent). Peptides were chromatographically separated at a constant flow rate of 250
362 nL/min using the following gradient: 3-4% solvent B (0.1% formic acid in 80 % acetonitrile) within 1.0
363 min, 4-27% solvent B within 119.0 min, 27-50% solvent B within 19.0 min, 50-95% solvent B within 1.0
364 min, followed by washing and column equilibration. The mass spectrometer was operated in data-
365 dependent acquisition mode. The MS1 survey scan was acquired from 300-1750 m/z at a resolution of
366 70,000. The top 10 most abundant peptides were isolated within a 1.8 Th window and subjected to
367 HCD fragmentation at a normalized collision energy of 27%. The AGC target was set to 5e5 charges,
368 allowing a maximum injection time of 55 ms. Product ions were detected in the Orbitrap at a resolution
369 of 17,500. Precursors were dynamically excluded for 30.0 s.
370 All mass spectrometric raw data were processed with Maxquant (version 1.5.3.8) using default
371 parameters. Briefly, MS2 spectra were searched against the canonical Uniprot mouse fasta database
372 (UP000000589; May 4, 2020) and the MaxQuant default list of common contaminants. False discovery
373 rates on protein and PSM level were estimated by the target-decoy approach to 1% (Protein FDR) and
374 1% (PSM FDR) respectively. The minimal peptide length was set to 7 amino acids and
375 carbamidomethylation at cysteine residues was considered as a fixed modification. Oxidation (M) and
376 Acetyl (Protein N-term) were included as variable modifications. The match-between runs option was
377 enabled. Student´s T-tests were calculated in Perseus (version 1.6.1.1) after removal of decoys and
378 potential contaminants. Data were filtered for at least 3 out of 3 values in at least one condition.

379 Remaining missing values were imputed with random values from the left end of the intensity
380 distribution using Perseus defaults.
381
382 Interactome analysis
383 For each replicate, a 10 cm dish of Jade1 KO1 mIMCD3 cells was transfected with 10 µg of either Flag-
384 tagged Jade1S, Jade1L or an empty vector control using Lipofectamine (Invitrogen) 2000 following the
385 manufacture's instructions. 48 h after transfection cells were harvested and lyzed (50 mM Tris (pH 7.5),
386 150 mM NaCl, 0.5% (w/v) Sodium deoxycholate, 1% (v/v) Triton X-100) for 15 min @ 4°C. After
387 sonication (Bioruptor, 10 min, cycle 30/30 sec) and centrifugation (4°C, 15 min) anti-FLAG agarose
388 beads (M2, Sigma) were added to the supernatant and incubated at 4°C overnight. After extensive
389 washing of the beads, 5% SDS in 1xPBS was added and proteins were released from the beads by
390 incubation at 95°C for 3 min. Subsequently, the supernatant was reduced with DTT and alkylated with
391 CAA followed by two single-pot solid-phase-enhanced sample preparations (SP3).
392 All samples were analyzed on a Q Exactive Plus Orbitrap (Thermo Scientific) mass spectrometer that
393 was coupled to an EASY nLC (Thermo Scientific). Peptides were loaded with solvent A (0.1% formic acid
394 in water) onto an in-house packed analytical column (50 cm — 75 µm I.D., filled with 2.7 µm Poroshell
395 EC120 C18, Agilent). Peptides were chromatographically separated at a constant flow rate of 250
396 nL/min using the following gradient: 3-5% solvent B (0.1% formic acid in 80 % acetonitrile) within 1.0
397 min, 5-30% solvent B within 65.0 min, 30-50% solvent B within 13.0 min, 50-95% solvent B within 1.0
398 min, followed by washing and column equilibration. The mass spectrometer was operated in data-
399 dependent acquisition mode. The MS1 survey scan was acquired from 300-1750 m/z at a resolution of
400 70,000. The top 10 most abundant peptides were isolated within a 1.8 Th window and subjected to
401 HCD fragmentation at a normalized collision energy of 27%. The AGC target was set to 5e5 charges,
402 allowing a maximum injection time of 110 ms. Product ions were detected in the Orbitrap at a
403 resolution of 35,000. Precursors were dynamically excluded for 15.0 s.
404 All mass spectrometric raw data were processed with Maxquant (version 1.5.3.8) using default
405 parameters. Briefly, MS2 spectra were searched against the canonical Uniprot
406 MOUSE_UP000000589.fasta (downloaded at: 26.08.2020) database, including a list of common
407 contaminants. False discovery rates on protein and PSM level were estimated by the target-decoy
408 approach to 1% (Protein FDR) and 1% (PSM FDR) respectively. The minimal peptide length was set to
409 7 amino acids and carbamidomethylation at cysteine residues was considered as a fixed modification.
410 Oxidation (M) and Acetyl (Protein N-term) were included as variable modifications. The match-
411 between runs option was enabled for replicates from the same group. LFQ quantification was enabled
412 using default settings.
413

414 *In vitro assay of 26S proteasome activity*

415 The proteasomal activity assay was performed as previously described (46). For each replicate with the
416 mIMCD3 cells, the cells were grown into 6-well plates and grown until 70% confluency. HEK29T cells
417 were grown into 6-well plates, transfected at 50% confluency with 2 µg of DNA using the calcium
418 phosphate method, and harvested 24 h after transfection. Cells were collected on proteasomal activity
419 assay buffer (50 mM Tris-HCL, pH 7.5, 10% glycerol, 5 mM $MgCl_2$, 0.5 mM EDTA, 2 mM ATP, 1 mM DTT)
420 and immediately frozen in liquid nitrogen. Before performing the assay, samples were lyzed and
421 centrifuged at 10000 g for 10 min at 4°C. 25 µg of protein was loaded on a flat-bottom, black
422 fluorescence 96-well microplate and incubated with the fluorogenic substrate (Z-Gly-Gly-Leu-AMC,
423 BML-ZW8505-0005, ENZO Life Science). Fluorescence (360 nm excitation, 430 nm emission) was
424 monitored every 5 min for 2 h at 37°C using a fluorescent plate reader (EnSpire Multimode Plate
425 Reader, Perkin Elmer). Samples were assayed in technical triplicates and in biological replicates as
426 indicated in the figure legend.

427

428 *mRNA sequencing*

429 Total RNA extraction was performed with the direct-zol RNA Miniprep kit (Zymo Research) following
430 the manufacture's instructions. Library preparation and sequencing was performed by the Cologne
431 Center for Genomics. Libraries were prepared using the Illumina® TruSeq® mRNA stranded sample
432 preparation Kit. Library preparation started with 300 ng total RNA. After poly-A selection, mRNA was
433 purified and fragmented using divalent cations under elevated temperature. The RNA fragments
434 underwent reverse transcription using random primers, followed by second strand cDNA synthesis
435 with DNA Polymerase I and RNase H. After end repair and A-tailing, indexing adapters were ligated.
436 The products were then purified and amplified to create the final cDNA libraries. After library validation
437 and quantification (TapStation 4200, Agilent), equimolar amounts of library were pooled and
438 quantified by using the Peqlab KAPA Library Quantification Kit and the Applied Biosystems 7900HT
439 Sequence Detection System. The pool was sequenced on an Illumina NovaSeq6000 with PE100 read
440 length and a minimum of 35 million reads per sample.

441 The reads were trimmed with Trimmomatic version 0.36 (47) using default parameters. The trimmed
442 reads were mapped to the GRCm39 mouse reference genome with STAR version 2.6 (48) using default
443 parameters. mRNA expression was analyzed using DESeq2 (version 1.28.1)(49) package of R (version
444 4.0.0) software (https://www.R-project.org/). A p-value cut-off of <0.05 was applied to the list of
445 differentially regulated mRNAs after pairwise comparison of the Jade deficient cell lines with wild type.
446 P-values were adjusted for multiple testing.

447

448

449 *Raw data deposition*

450 The proteome and interactome mass spectrometry proteomics data have been deposited to the
451 ProteomeXchange Consortium (http://proteomecentral.proteomexchange.org) via the PRIDE partner
452 repository (50) with the dataset identifier PXD028800. RNA sequencing data have been deposited in
453 the ArrayExpress database at EMBL-EBI (www.ebi.ac.uk/arrayexpress) under accession number E-
454 MTAB-11021 (51). Login information are available upon request.

455

456 **References**

457 1. Zhou, M. I., Wang, H., Ross, J. J., Kuzmin, I., Xu, C., and Cohen, H. T. (2002) The von Hippel-
458 Lindau tumor suppressor stabilizes novel plant homeodomain protein Jade-1. *J. Biol. Chem.*
459 **277**, 39887–39898
460 2. Foster, K., Prowse, A., van den Berg, A., Fleming, S., Hulsbeek, M. M., Crossey, P. A., Richards, F.
461 M., Cairns, P., Affara, N. A., and Ferguson-Smith, M. A. (1994) Somatic mutations of the von
462 Hippel-Lindau disease tumour suppressor gene in non-familial clear cell renal carcinoma. *Hum*
463 *Mol Genet*. **3**, 2169–2173
464 3. Gnarra, J. R., Tory, K., Weng, Y., Schmidt, L., Wei, M. H., Li, H., Latif, F., Liu, S., Chen, F., and Duh,
465 F. M. (1994) Mutations of the VHL tumour suppressor gene in renal carcinoma. *Nat Genet*. **7**,
466 85–90
467 4. Shuin, T., Kondo, K., Torigoe, S., Kishida, T., Kubota, Y., Hosaka, M., Nagashima, Y., Kitamura, H.,
468 Latif, F., and Zbar, B. (1994) Frequent somatic mutations and loss of heterozygosity of the von
469 Hippel-Lindau tumor suppressor gene in primary human renal cell carcinomas. *Cancer Res*. **54**,
470 2852–2855
471 5. Whaley, J. M., Naglich, J., Gelbert, L., Hsia, Y. E., Lamiell, J. M., Green, J. S., Collins, D.,
472 Neumann, H. P. H., Laidlaw, J., Li, F. P., Klein-Szanto, A. J. P., Seizinger, B. R., and Kley, N. (1994)
473 Germ-Line Mutations in the von Hippel–Lindau Tumor-Suppressor Gene Are Similar to Somatic
474 von Hippel–Lindau Aberrations in Sporadic Renal Cell Carcinoma. *Am J Hum Genet*. **55**, 1092–
475 1102
476 6. Zeng, L., Bai, M., Mittal, A. K., El-Jouni, W., Zhou, J., Cohen, D. M., Zhou, M. I., and Cohen, H. T.
477 (2013) Candidate tumor suppressor and pVHL partner Jade-1 binds and inhibits AKT in renal cell
478 carcinoma. *Cancer Res.* **73**, 5371–5380
479 7. Zhou, M. I., Wang, H., Foy, R. L., Ross, J. J., and Cohen, H. T. (2004) Tumor suppressor von
480 Hippel-Lindau (VHL) stabilization of Jade-1 protein occurs through plant homeodomains and is
481 VHL mutation dependent. *Cancer Res.* **64**, 1278–1286
482 8. Zhou, M. I., Foy, R. L., Chitalia, V. C., Zhao, J., Panchenko, M. V., Wang, H., and Cohen, H. T.
483 (2005) Jade-1, a candidate renal tumor suppressor that promotes apoptosis. *Proc. Natl. Acad.*
484 *Sci. U.S.A.* **102**, 11035–11040
485 9. Chitalia, V. C., Foy, R. L., Bachschmid, M. M., Zeng, L., Panchenko, M. V., Zhou, M. I., Bharti, A.,
486 Seldin, D. C., Lecker, S. H., Dominguez, I., and Cohen, H. T. (2008) Jade-1 inhibits Wnt signalling
487 by ubiquitylating beta-catenin and mediates Wnt pathway inhibition by pVHL. *Nat. Cell Biol.* **10**,
488 1208–1216
489 10. Benzing, T., and Schermer, B. (2012) Clinical spectrum and pathogenesis of nephronophthisis.
490 *Current Opinion in Nephrology and Hypertension*. **21**, 272–278
491 11. Borgal, L., Habbig, S., Hatzold, J., Liebau, M. C., Dafinger, C., Sacarea, I., Hammerschmidt, M.,
492 Benzing, T., and Schermer, B. (2012) The ciliary protein nephrocystin-4 translocates the
493 canonical Wnt regulator Jade-1 to the nucleus to negatively regulate β-catenin signaling. *J. Biol.*
494 *Chem.* **287**, 25370–25380
495 12. Foy, R. L., Chitalia, V. C., Panchenko, M. V., Zeng, L., Lopez, D., Lee, J. W., Rana, S. V., Boletta, A.,
496 Qian, F., Tsiokas, L., Piontek, K. B., Germino, G. G., Zhou, M. I., and Cohen, H. T. (2012)

Polycystin-1 regulates the stability and ubiquitination of transcription factor Jade-1. *Hum. Mol. Genet.* **21**, 5456–5471

13. Hildebrandt, F., Benzing, T., and Katsanis, N. (2011) Ciliopathies. *N Engl J Med*. **364**, 1533–1543
14. Foy, R. L., Song, I. Y., Chitalia, V. C., Cohen, H. T., Saksouk, N., Cayrou, C., Vaziri, C., Côté, J., and Panchenko, M. V. (2008) Role of Jade-1 in the histone acetyltransferase (HAT) HBO1 complex. *J. Biol. Chem.* **283**, 28817–28826
15. Panchenko, M. V., Zhou, M. I., and Cohen, H. T. (2004) von Hippel-Lindau partner Jade-1 is a transcriptional co-activator associated with histone acetyltransferase activity. *J. Biol. Chem.* **279**, 56032–56041
16. Johmura, Y., Osada, S., Nishizuka, M., and Imagawa, M. (2008) FAD24 acts in concert with histone acetyltransferase HBO1 to promote adipogenesis by controlling DNA replication. *J Biol Chem*. **283**, 2265–2274
17. Quintela, M., Sieglaff, D. H., Gazze, A. S., Zhang, A., Gonzalez, D., Francis, L., Webb, P., and Conlan, R. S. (2019) HBO1 directs histone H4 specific acetylation, potentiating mechano-transduction pathways and membrane elasticity in ovarian cancer cells. *Nanomedicine*. **17**, 254–265
18. Tzouanacou, E., Tweedie, S., and Wilson, V. (2003) Identification of Jade1, a gene encoding a PHD zinc finger protein, in a gene trap mutagenesis screen for genes involved in anteroposterior axis development. *Mol Cell Biol*. **23**, 8553–8552
19. Panchenko, M. V. (2016) Structure, function and regulation of jade family PHD finger 1 (JADE1). *Gene*. **589**, 1–11
20. Han, X., Gui, B., Xiong, C., Zhao, L., Liang, J., Sun, L., Yang, X., Yu, W., Si, W., Yan, R., Yi, X., Zhang, D., Li, W., Li, L., Yang, J., Wang, Y., Sun, Y. E., Zhang, D., Meng, A., and Shang, Y. (2014) Destabilizing LSD1 by Jade-2 promotes neurogenesis: an antibraking system in neural development. *Mol. Cell*. **55**, 482–494
21. Wu, C.-Y., Persaud, S. D., and Wei, L.-N. (2016) Retinoic Acid Induces Ubiquitination-Resistant RIP140/LSD1 Complex to Fine-Tune Pax6 Gene in Neuronal Differentiation. *Stem Cells*. **34**, 114–123
22. Anan, K., Hino, S., Shimizu, N., Sakamoto, A., Nagaoka, K., Takase, R., Kohrogi, K., Araki, H., Hino, Y., Usuki, S., Oki, S., Tanaka, H., Nakamura, K., Endo, F., and Nakao, M. (2018) LSD1 mediates metabolic reprogramming by glucocorticoids during myogenic differentiation. *Nucleic Acids Res*. **46**, 5441–5454
23. Jian, Y., Wang, M., Zhang, Y., Ou, R., Zhu, Z., Ou, Y., Chen, X., Liang, X., Ding, Y., Song, L., Xu, X., and Liao, W. (2018) Jade family PHD finger 3 (JADE3) increases cancer stem cell-like properties and tumorigenicity in colon cancer. *Cancer Letters*. **428**, 1–11
24. Doyon, Y., Cayrou, C., Ullah, M., Landry, A.-J., Côté, V., Selleck, W., Lane, W. S., Tan, S., Yang, X.-J., and Côté, J. (2006) ING tumor suppressor proteins are critical regulators of chromatin acetylation required for genome expression and perpetuation. *Mol Cell*. **21**, 51–64
25. Yates, A. D., Achuthan, P., Akanni, W., Allen, J., Allen, J., Alvarez-Jarreta, J., Amode, M. R., Armean, I. M., Azov, A. G., Bennett, R., Bhai, J., Billis, K., Boddu, S., Marugán, J. C., Cummins, C., Davidson, C., Dodiya, K., Fatima, R., Gall, A., Giron, C. G., Gil, L., Grego, T., Haggerty, L., Haskell, E., Hourlier, T., Izuogu, O. G., Janacek, S. H., Juettemann, T., Kay, M., Lavidas, I., Le, T., Lemos, D., Martinez, J. G., Maurel, T., McDowall, M., McMahon, A., Mohanan, S., Moore, B., Nuhn, M., Oheh, D. N., Parker, A., Parton, A., Patricio, M., Sakthivel, M. P., Abdul Salam, A. I., Schmitt, B. M., Schuilenburg, H., Sheppard, D., Sycheva, M., Szuba, M., Taylor, K., Thormann, A., Threadgold, G., Vullo, A., Walts, B., Winterbottom, A., Zadissa, A., Chakiachvili, M., Flint, B., Frankish, A., Hunt, S. E., IIsley, G., Kostadima, M., Langridge, N., Loveland, J. E., Martin, F. J., Morales, J., Mudge, J. M., Muffato, M., Perry, E., Ruffier, M., Trevanion, S. J., Cunningham, F., Howe, K. L., Zerbino, D. R., and Flicek, P. (2020) Ensembl 2020. *Nucleic Acids Research*. **48**, D682–D688

547 26. Park, J., Shrestha, R., Qiu, C., Kondo, A., Huang, S., Werth, M., Li, M., Barasch, J., and Suszták, K.
548 (2018) Single-cell transcriptomics of the mouse kidney reveals potential cellular targets of
549 kidney disease. *Science*. **360**, 758–763
550 27. Borgal, L., Rinschen, M. M., Dafinger, C., Hoff, S., Reinert, M. J., Lamkemeyer, T., Lienkamp, S.
551 S., Benzing, T., and Schermer, B. (2014) Casein kinase 1 α phosphorylates the Wnt regulator
552 Jade-1 and modulates its activity. *J. Biol. Chem.* **289**, 26344–26356
553 28. Borgal, L., Rinschen, M. M., Dafinger, C., Liebrecht, V. I., Abken, H., Benzing, T., and Schermer,
554 B. (2016) Jade-1S phosphorylation induced by CK1α contributes to cell cycle progression. *Cell*
555 *Cycle*. **15**, 1034–1045
556 29. Lian, X., Duan, X., Wu, X., Li, C., Chen, S., Wang, S., Cai, Y., and Weng, Z. (2012) Expression and
557 clinical significance of von Hippel-Lindau downstream genes: Jade-1 and β-catenin related to
558 renal cell carcinoma. *Urology*. **80**, 485.e7–13
559 30. Xiao-Fen, W., Ting, C., Jie, L., Deng-Yang, M., Qing-Feng, Z., and Xin, L. (2016) Correlation
560 analysis of VHL and Jade-1 gene expression in human renal cell carcinoma. *Open Med (Wars)*.
561 **11**, 226–230
562 31. Havasi, A., Haegele, J. A., Gall, J. M., Blackmon, S., Ichimura, T., Bonegio, R. G., and Panchenko,
563 M. V. (2013) Histone acetyl transferase (HAT) HBO1 and JADE1 in epithelial cell regeneration.
564 *Am. J. Pathol.* **182**, 152–162
565 32. Fedeles, S. V., Tian, X., Gallagher, A.-R., Mitobe, M., Nishio, S., Lee, S. H., Cai, Y., Geng, L., Crews,
566 C. M., and Somlo, S. (2011) A genetic interaction network of five genes for human polycystic
567 kidney and liver diseases defines polycystin-1 as the central determinant of cyst formation. *Nat*
568 *Genet*. **43**, 639–647
569 33. Asawa, R. R., Danchik, C., Zahkarov, A., Chen, Y., Voss, T., Jadhav, A., Wallace, D. P., Trott, J. F.,
570 Weiss, R. H., Simeonov, A., and Martinez, N. J. (2020) A high-throughput screening platform for
571 Polycystic Kidney Disease (PKD) drug repurposing utilizing murine and human ADPKD cells.
572 *Scientific reports*. **10**, 4203
573 34. Kim, J. H., Ki, S. M., Joung, J.-G., Scott, E., Heynen-Genel, S., Aza-Blanc, P., Kwon, C. H., Kim, J.,
574 Gleeson, J. G., and Lee, J. E. (2016) Genome-wide screen identifies novel machineries required
575 for both ciliogenesis and cell cycle arrest upon serum starvation. *Biochim Biophys Acta*. **1863**,
576 1307–1318
577 35. Sang, L., Miller, J. J., Corbit, K. C., Giles, R. H., Brauer, M. J., Otto, E. A., Baye, L. M., Wen, X.,
578 Scales, S. J., Kwong, M., Huntzicker, E. G., Sfakianos, M. K., Sandoval, W., Bazan, J. F., Kulkarni,
579 P., Garcia-Gonzalo, F. R., Seol, A. D., O'Toole, J. F., Held, S., Reutter, H. M., Lane, W. S., Rafiq, M.
580 A., Noor, A., Ansar, M., Devi, A. R. R., Sheffield, V. C., Slusarski, D. C., Vincent, J. B., Doherty, D.
581 A., Hildebrandt, F., Reiter, J. F., and Jackson, P. K. (2011) Mapping the Nephronophthisis-
582 Joubert-Meckel-Gruber Protein Network Reveals Ciliopathy Disease Genes and Pathways. *Cell*.
583 **145**, 513–528
584 36. Liu, Y. P., Tsai, I.-C., Morleo, M., Oh, E. C., Leitch, C. C., Massa, F., Lee, B.-H., Parker, D. S., Finley,
585 D., Zaghloul, N. A., Franco, B., and Katsanis, N. (2014) Ciliopathy proteins regulate paracrine
586 signaling by modulating proteasomal degradation of mediators. *J Clin Invest*. **124**, 2059–2070
587 37. Ma, M., Tian, X., Igarashi, P., Pazour, G. J., and Somlo, S. (2013) Loss of cilia suppresses cyst
588 growth in genetic models of autosomal dominant polycystic kidney disease. *Nat Genet*. **45**,
589 1004–1012
590 38. Schermer, B., Ghenoiu, C., Bartram, M., Müller, R. U., Kotsis, F., Höhne, M., Kühn, W., Rapka,
591 M., Nitschke, R., Zentgraf, H., Fliegauf, M., Omran, H., Walz, G., and Benzing, T. (2006) The von
592 Hippel-Lindau tumor suppressor protein controls ciliogenesis by orienting microtubule growth.
593 *J Cell Biol*. **175**, 547–554
594 39. Ran, F. A., Hsu, P. D., Wright, J., Agarwala, V., Scott, D. A., and Zhang, F. (2013) Genome
595 engineering using the CRISPR-Cas9 system. *Nature Protocols*. **8**, 2281–2308
596 40. Hodgkins, A., Farne, A., Perera, S., Grego, T., Parry-Smith, D. J., Skarnes, W. C., and Iyer, V.
597 (2015) WGE: a CRISPR database for genome engineering. *Bioinformatics*. **31**, 3078–3080

598 41. Rauniyar, N. (2015) Parallel Reaction Monitoring: A Targeted Experiment Performed Using High
599 Resolution and High Mass Accuracy Mass Spectrometry. *Int J Mol Sci*. **16**, 28566–28581
600 42. Bartram, M. P., Habbig, S., Pahmeyer, C., Höhne, M., Weber, L. T., Thiele, H., Altmüller, J.,
601 Kottoor, N., Wenzel, A., Krueger, M., Schermer, B., Benzing, T., Rinschen, M. M., and Beck, B. B.
602 (2016) Three-layered proteomic characterization of a novel ACTN4 mutation unravels its
603 pathogenic potential in FSGS. *Hum Mol Genet*. **25**, 1152–1164
604 43. Gessulat, S., Schmidt, T., Zolg, D. P., Samaras, P., Schnatbaum, K., Zerweck, J., Knaute, T.,
605 Rechenberger, J., Delanghe, B., Huhmer, A., Reimer, U., Ehrlich, H.-C., Aiche, S., Kuster, B., and
606 Wilhelm, M. (2019) Prosit: proteome-wide prediction of peptide tandem mass spectra by deep
607 learning. *Nat Methods*. **16**, 509–518
608 44. MacLean, B., Tomazela, D. M., Shulman, N., Chambers, M., Finney, G. L., Frewen, B., Kern, R.,
609 Tabb, D. L., Liebler, D. C., and MacCoss, M. J. (2010) Skyline: an open source document editor
610 for creating and analyzing targeted proteomics experiments. *Bioinformatics*. **26**, 966–968
611 45. Pino, L. K., Searle, B. C., Bollinger, J. G., Nunn, B., MacLean, B., and MacCoss, M. J. (2020) The
612 Skyline ecosystem: Informatics for quantitative mass spectrometry proteomics. *Mass Spectrom*
613 *Rev*. **39**, 229–244
614 46. Kisselev, A. F., and Goldberg, A. L. (2005) Monitoring Activity and Inhibition of 26S Proteasomes
615 with Fluorogenic Peptide Substrates. in *Methods in Enzymology*, pp. 364–378, Ubiquitin and
616 Protein Degradation, Part A, Academic Press, **398**, 364–378
617 47. Bolger, A. M., Lohse, M., and Usadel, B. (2014) Trimmomatic: a flexible trimmer for Illumina
618 sequence data. *Bioinformatics*. **30**, 2114–2120
619 48. Dobin, A., Davis, C. A., Schlesinger, F., Drenkow, J., Zaleski, C., Jha, S., Batut, P., Chaisson, M.,
620 and Gingeras, T. R. (2013) STAR: ultrafast universal RNA-seq aligner. *Bioinformatics*. **29**, 15–21
621 49. Love, M. I., Huber, W., and Anders, S. (2014) Moderated estimation of fold change and
622 dispersion for RNA-seq data with DESeq2. *Genome Biology*. **15**, 550
623 50. Perez-Riverol, Y., Csordas, A., Bai, J., Bernal-Llinares, M., Hewapathirana, S., Kundu, D. J.,
624 Inuganti, A., Griss, J., Mayer, G., Eisenacher, M., Pérez, E., Uszkoreit, J., Pfeuffer, J.,
625 Sachsenberg, T., Yilmaz, S., Tiwary, S., Cox, J., Audain, E., Walzer, M., Jarnuczak, A. F., Ternent,
626 T., Brazma, A., and Vizcaíno, J. A. (2019) The PRIDE database and related tools and resources in
627 2019: improving support for quantification data. *Nucleic Acids Res*. **47**, D442–D450
628 51. Athar, A., Füllgrabe, A., George, N., Iqbal, H., Huerta, L., Ali, A., Snow, C., Fonseca, N. A.,
629 Petryszak, R., Papatheodorou, I., Sarkans, U., and Brazma, A. (2019) ArrayExpress update – from
630 bulk to single-cell expression data. *Nucleic Acids Research*. **47**, D711–D715
631 52. Rice, P., Longden, I., and Bleasby, A. (2000) EMBOSS: the European Molecular Biology Open
632 Software Suite. *Trends Genet*. **16**, 276–277
633 53. Letunic, I., and Bork, P. (2018) 20 years of the SMART protein domain annotation resource.
634 *Nucleic Acids Res*. **46**, D493–D496
635 54. Oughtred, R., Rust, J., Chang, C., Breitkreutz, B.-J., Stark, C., Willems, A., Boucher, L., Leung, G.,
636 Kolas, N., Zhang, F., Dolma, S., Coulombe-Huntington, J., Chatr-Aryamontri, A., Dolinski, K., and
637 Tyers, M. (2021) The BioGRID database: A comprehensive biomedical resource of curated
638 protein, genetic, and chemical interactions. *Protein Sci*. **30**, 187–200
639 55. Consortium, T. U. (2019) UniProt: a worldwide hub of protein knowledge. *Nucleic Acids Res*. **47**,
640 D506–D515
641 56. Madeira F, Park Ym, Lee J, Buso N, Gur T, Madhusoodanan N, Basutkar P, Tivey Arn, Potter Sc,
642 Finn Rd, and Lopez R (2019) The EMBL-EBI search and sequence analysis tools APIs in 2019.
643 *Nucleic Acids Res*. **47**, W636–W641
644 57. Uhlén, M., Fagerberg, L., Hallström, B. M., Lindskog, C., Oksvold, P., Mardinoglu, A., Sivertsson,
645 Å., Kampf, C., Sjöstedt, E., Asplund, A., Olsson, I., Edlund, K., Lundberg, E., Navani, S., Szigyarto,
646 C. A.-K., Odeberg, J., Djureinovic, D., Takanen, J. O., Hober, S., Alm, T., Edqvist, P.-H., Berling, H.,
647 Tegel, H., Mulder, J., Rockberg, J., Nilsson, P., Schwenk, J. M., Hamsten, M., Feilitzen, K. von,
648 Forsberg, M., Persson, L., Johansson, F., Zwahlen, M., Heijne, G. von, Nielsen, J., and Pontén, F.
649 (2015) Tissue-based map of the human proteome. *Science*. 10.1126/science.1260419

650 **Figure legends**

651 **Figure 1: All JADE protein family members co-precipitate with the ciliopathy proteins NPHP1, NPHP4,**
652 **and pVHL**. **(A)** Domain structure of the human JADE proteins. PHD – Cys4HisCys3 plant homeo domain;
653 NLS – nuclear localization signal; PEST – protein degradation amino acid sequence. Domain information
654 obtained from EMBOSS/epestfind (52), SMART(53), and NLS prediction (consensus sequence K – (K/R)
655 –X – (K/R)). **(B-D)** HEK293T cells were transiently transfected with **(B)** V5-tagged pVHL (V5.VHL), **(C)**
656 V5-tagged Nphp4 (V5.NPHP4), and **(D)** V5-tagged Nphp1 (V5.NHPH1), and either FLAG-tagged JADE1S
657 (F.JADE1S), Jade2 (F.JADE2), Jade3 (F.JADE3) or a control protein (F.EPS$^{1-225}$). Immunoprecipitates with
658 an anti-FLAG antibody were analyzed by immunoblotting with antibodies (anti-V5; anti-FLAG) as
659 indicated. V5.VHL, V5.NPHP1, and V5.NPHP4 all coimmunoprecipitate with F.Jade1S/2/3 but not with
660 F.EPS$^{1-225}$. Blots are representative for at least three independent experiments. **(E,F)** HEK293T cells
661 were transiently cotransfected with **(E)** V5.JADE1S and FLAG.JADE1S or **(F)** V5.JADE2 and FLAG.JADE2.
662 FLAG.pVHL and FLAG.EPS$^{1-225}$ served as positive and negative control, respectively.
663 Immunoprecipitates with an anti-FLAG antibody were analyzed by immunoblotting with antibodies as
664 indicated. V5.JADE1S and V5.JADE2 both coimmunoprecipitate with the respective FLAG-tagged JADE
665 protein. **(G)** HEK293T cells were transiently transfected with V5.JADE2 and either FLAG-tagged JADE1S,
666 JADE3, pVHL, or EPS$^{1-225}$. Immunoprecipitates with an anti-FLAG antibody were analyzed by
667 immunoblotting with antibodies (anti-V5; anti-FLAG) as indicated. V5.JADE2 coimmunoprecipitate
668 with F.JADE1S, F.JADE3, and F.VHL but not with F.EPS$^{1-225}$ (h.c.: heavy chain, l.c.: light chain).

669 **Figure 2: Deletion of one specific Jade protein does affect neither transcription nor expression of the**
670 **remaining family members. (A-C)** qPCR data comparing the expression fold change of each targeted
671 gene across the different cell lines. Only the expression of the targeted gene in the respective mutant
672 cell lines is significantly reduced, while the other Jade mRNAs are not significantly altered. (N=3,
673 students t-test, * $p \leq 0.05$, ** $p \leq 0.01$, *** $p \leq 0.001$) **(D-F)** Parallel reaction monitoring (PRM) assay
674 for **(D)** Jade1, **(E)** Jade2, and **(F)** Jade3 comparing the peak areas for the selected peptides across
675 mIMCD3 WT and Jade mutant cell lines for protein quantification. The localization of peptides selected
676 for PRM assay is depicted above the bar charts. (N=3)

677 **Figure 3: Proteomic analysis reveals upregulation of the proteasome in cell lines lacking either one**
678 **of the Jade family members**. (A-C) Principal component analysis (PCA) plot of the protein expression
679 data of WT, Jade1 (A), Jade2 (B), and Jade3 (C) KO1 and KO2 cell lines. Depicted are the first two
680 principal components (PC1 and PC2). The axes represent the percentages of variation explained by the
681 principal components. The replicates of the different groups cluster together and the difference
682 between mutant and wildtype groups explains the largest variance. (D) Venn diagram depicting the
683 overlap between significantly regulated proteins across the Jade-deficient cell lines. The Jade1 section
684 includes all proteins that are significantly regulated (p-value < 0.05) in either one or both of the Jade1-

685 deficient cell lines. The Jade2 and Jade3 sections generated in the same way. (E) GO and KEGG pathway
686 annotation based on a Fisher exact test of the 644 proteins found to be regulated in all Jade mutant
687 cell lines. (F) Representative scatter plot with the t-test differences in protein expression of the Jade1
688 KO2 mutant cells vs the wildtype cells on the x-axis and the statistical significance (-$\log_{10}$ Student's t-
689 test p-value) on the y-axis. Proteins associated with the ubiquitin proteasome system are highlighted
690 in magenta. (G) Heatmap of the proteins highlighted in (F) based on logarithmized LFQ values for all
691 Jade-deficient cell lines and the control line visualizing the upregulation of proteasome-associated
692 proteins.
693 **Figure 4: Increased proteasome activity observed in Jade-deficient cell lines. (A)** Measurement of the
694 proteasome activity in wildtype and Jade-deficient mIMCD3 cell lines. The proteasome activity of
695 Jade1, Jade2, or Jade3-deficient cell lines is increased compared to the wildtype control.
696 Quantification of the slope as readout for proteasome activity (N=3, one-way ANOVA with Dunnett's
697 post-hoc test, ****$p \leq 0.0001$) **(B)** Measurement of the proteasome activity in HEK293T cell with either
698 Jade1S, Jade1L, Jade2, Jade3, or Podocin (control) overexpressed. All cell lines with overexpressed Jade
699 proteins show a decreased activity compared to the control with only Jade1S/L reaching statistical
700 significance. Quantification of the slope as readout for proteasome activity (N=3, one-way ANOVA
701 Dunnett's post-hoc test, * $p \leq 0.05$)
702 **Figure 5: Interactome analysis reveals a link between Jade1L/S proteins and proteasomal**
703 **components. (A)** Jade1 KO1 mIMCD3 cells were transiently transfected with either Flag-tagged Jade1L,
704 Jade1S, or a control plasmid. Pulldown was performed with anti-Flag (M2) sepharose beads. Heatmap
705 of average iBAQ values for proteins which were never measured in the control samples, but in either
706 all replicates for Jade1L, all replicated for Jade1S, or all replicates of both. The protein with the highest
707 iBAQ is Jade1 for both, the Jade1S and the Jade1L pulldown. **(B/C)**
708 Quantitative analysis of the Jade1L **(B)** & Jade1S **(C)** interactome. Proteins on the right side, above the
709 p=0.05 line, are determined significantly enriched. Proteasomal components are highlighted in
710 magenta, known JADE1/Jade1 interactors based on known interactors annotated in BioGrid (54) in
711 green.
712
713 **Supplementary Figure Legends**
714 **Supplemental Figure S1: Sequence alignment and expression profiles of the JADE protein family**
715 **members.** (A) Protein identity matrix for human and mouse JADE family paralogues. Protein sequences
716 were obtained from Uniprot (55) and the identity score was calculated using Clustal Omega (56). (B)
717 Protein Expression Levels for JADE1 across different tissues. Based on tissue micro arrays obtained
718 from The Human Protein Atlas version 19.3 and Ensembl version 92.38. Proteomic data available from
719 https://v19.proteinatlas.org/download/normal_tissue.tsv.zip . (57). (C) RNA expression profiles across

720 different tissues for *JADE1/2/3*. Consensus transcript expression levels based on transcriptomic data
721 from HPA, GTEx and FANTOM5. Normalized expression (NX) based on the maximum NX for each gene
722 in the different data sets. Data is obtained from The Human Protein Atlas v 19.3 and Ensembl version
723 92.38. Transcriptomic data available from
724 https://v19.proteinatlas.org/download/rna_tissue_consensus.tsv.zip. (57). (D) Gene expression data
725 of single cell transcriptomics of mouse kidney. Shown is the percentage of cells expressing each *Jade*
726 gene in the different cell clusters: endothelial, vascular, and descending loop of Henle (Endo), podocyte
727 (Podo), proximal tubule (PT), ascending loop of Henle (LOH), distal convoluted tubule (DCT), collecting
728 duct principal cell (CD-PC), collecting duct intercalated cell (CD-IC), collecting duct transitional cell (CD-
729 Trans), fibroblast (Fib), macrophage (Macro), neutrophil (Neutro), lymphocyte (lymph), natural killer
730 cell (NK)(26).
731 **Supplemental figure S2: Generation and validation of Jade1/2/3 mIMCD3 mutant cell lines.** (A)
732 Selection of sgRNAs targeting exons containing the first and the second PHD domain. sgRNA selection
733 was based on location and off-target scores using Wellcome Sanger Institute Genome Editing
734 (https://wge.stemcell.sanger.ac.uk/) (40). (B) Sanger sequencing of mRNA confirms mutations.
735 **Supplemental figure S3: Protein turnover machinery is upregulated upon loss of Jade family**
736 **members. (A-C)** Comparison of the two different mutant cell lines for Jade1 **(A)**, Jade2 **(B)**, and Jade3
737 **(C)**. The fold change of KO1 is depicted on the x-axis, the fold change of the KO2 on the y-axis. Proteins
738 are highlighted according to their significance as indicated in the figure. **(D)** Scatter plot with the t-test
739 differences in protein expression of the Jade1 KO2 mutant cells vs the wildtype cells on the x-axis and
740 the statistical significance (-$\log_{10}$ Student's t-test p-value) on the y-axis. Ribosomal proteins are
741 highlighted in magenta, tRNA ligases in blue, and elongation factors in green. **(E, F)** Heatmap of the
742 proteins highlighted in (D) based on logarithmic LFQ values for all seven cell lines to visualize the
743 upregulation of ribosomal proteins (E), tRNA ligases, and elongation factors (F) across Jade-deficient
744 cell lines.
745 **Supplemental figure S4: Transcriptomic analysis reveals no major regulation of the proteasome. (A)**
746 PCA plot of the gene expression data of WT, *Jade1* KO1 and KO2 cell lines. Depicted are the first two
747 principal components (PC1 and PC2). The axes represent the percentages of variation explained by the
748 principal components. The replicates of the different groups cluster together and the difference
749 between mutant and wildtype groups explains the largest variance. PCA plots of *Jade2* **(B)** and *Jade3*
750 **(C)** cell lines show clustering of the groups. Here, the second component accounts for the difference
751 between mutant and wildtype cell lines. **(D-F)** Comparison of the two different mutant cell lines for
752 *Jade1* **(D)**, *Jade2* **(E)**, and *Jade3* **(F)**. The fold change of KO1 is depicted on the x-axis, the fold change of
753 the KO2 on the y-axis. Genes are highlighted according to their significance as indicated in the figure.

754 **Supplemental figure S5: Transcriptomic analysis reveals no major regulation of the proteasome. (A)**
755 Venn diagram depicting the overlap between significantly regulated genes across the *Jade*-deficient
756 cell lines. The *Jade1* section includes all proteins that are significantly regulated (p-value < 0.05) in
757 either one or both of the *Jade1*-deficient cell lines. The *Jade2* and *Jade3* sections generated in the same
758 way. **(B)** Scatter plot with the log2FoldChange in gene expression of the *Jade1* KO2 mutant cells vs the
759 wildtype cells on the x-axis and the statistical significance (-log adj. p-value) on the y-axis. Genes of
760 proteasomal components are highlighted in magenta. **(C)** Heatmap of the genes highlighted in (H)
761 based on logarithmic normalized counts for all seven cell lines to visualize that the proteasomal
762 components are not upregulated on a transcriptional level across Jade-deficient cell lines. **(D-F)**
763 Heatmap of ribosomal genes **(D)**, genes encoding for tRNA-ligases **(E)**, and genes encoding for
764 transcription initiation and elongation factors **(F)**. Logarithmic normalized counts for all seven cell lines
765 are shown.
766
767 **Supplemental tables**
768 Supplemental table S1: Primer sequences.
769 Supplemental table S2: Unique target peptides for PRM assay.
770
771
772
773
774
775
776
777
778
779
780
781
782
783
784
785
786
787

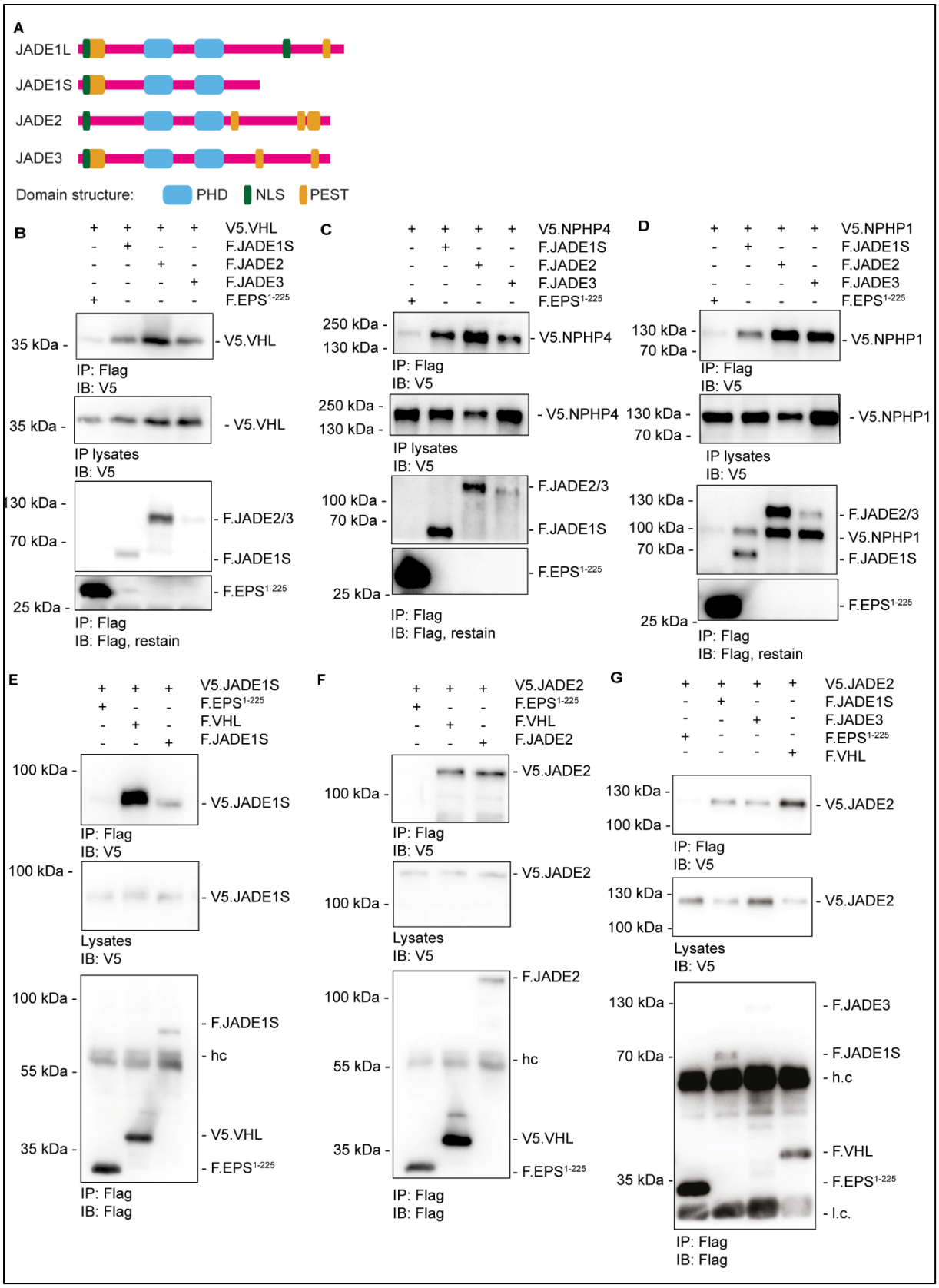

Figure 1: All JADE protein family members co-precipitate with the ciliopathy proteins NPHP1, NPHP4, and pVHL. (A) Domain structure of the human JADE proteins. PHD – Cys4HisCys3 plant homeo domain; NLS – nuclear localization signal; PEST – protein degradation amino acid sequence. Domain information obtained from EMBOSS/epestfind (52), SMART(53), and NLS prediction (consensus sequence K – (K/R)

793 –X – (K/R)). **(B-D)** HEK293T cells were transiently transfected with **(B)** V5-tagged pVHL (V5.VHL), **(C)**
794 V5-tagged Nphp4 (V5.NPHP4), and **(D)** V5-tagged Nphp1 (V5.NHPH1), and either FLAG-tagged JADE1S
795 (F.JADE1S), Jade2 (F.JADE2), Jade3 (F.JADE3) or a control protein (F.EPS$^{1-225}$). Immunoprecipitates with
796 an anti-FLAG antibody were analyzed by immunoblotting with antibodies (anti-V5; anti-FLAG) as
797 indicated. V5.VHL, V5.NPHP1, and V5.NPHP4 all coimmunoprecipitate with F.Jade1S/2/3 but not with
798 F.EPS$^{1-225}$. Blots are representative for at least three independent experiments. **(E,F)** HEK293T cells
799 were transiently co-transfected with **(E)** V5.JADE1S and FLAG.JADE1S or **(F)** V5.JADE2 and FLAG.JADE2.
800 FLAG.pVHL and FLAG.EPS$^{1-225}$ served as positive and negative control, respectively.
801 Immunoprecipitates with an anti-FLAG antibody were analyzed by immunoblotting with antibodies as
802 indicated. V5.JADE1S and V5.JADE2 both co-immunoprecipitate with the respective FLAG-tagged JADE
803 protein. **(G)** HEK293T cells were transiently transfected with V5.JADE2 and either FLAG-tagged JADE1S,
804 JADE3, pVHL, or EPS$^{1-225}$. Immunoprecipitates with an anti-FLAG antibody were analyzed by
805 immunoblotting with antibodies (anti-V5; anti-FLAG) as indicated. V5.JADE2 coimmunoprecipitate
806 with F.JADE1S, F.JADE3, and F.VHL but not with F.EPS$^{1-225}$ (h.c.: heavy chain, l.c.: light chain).
807

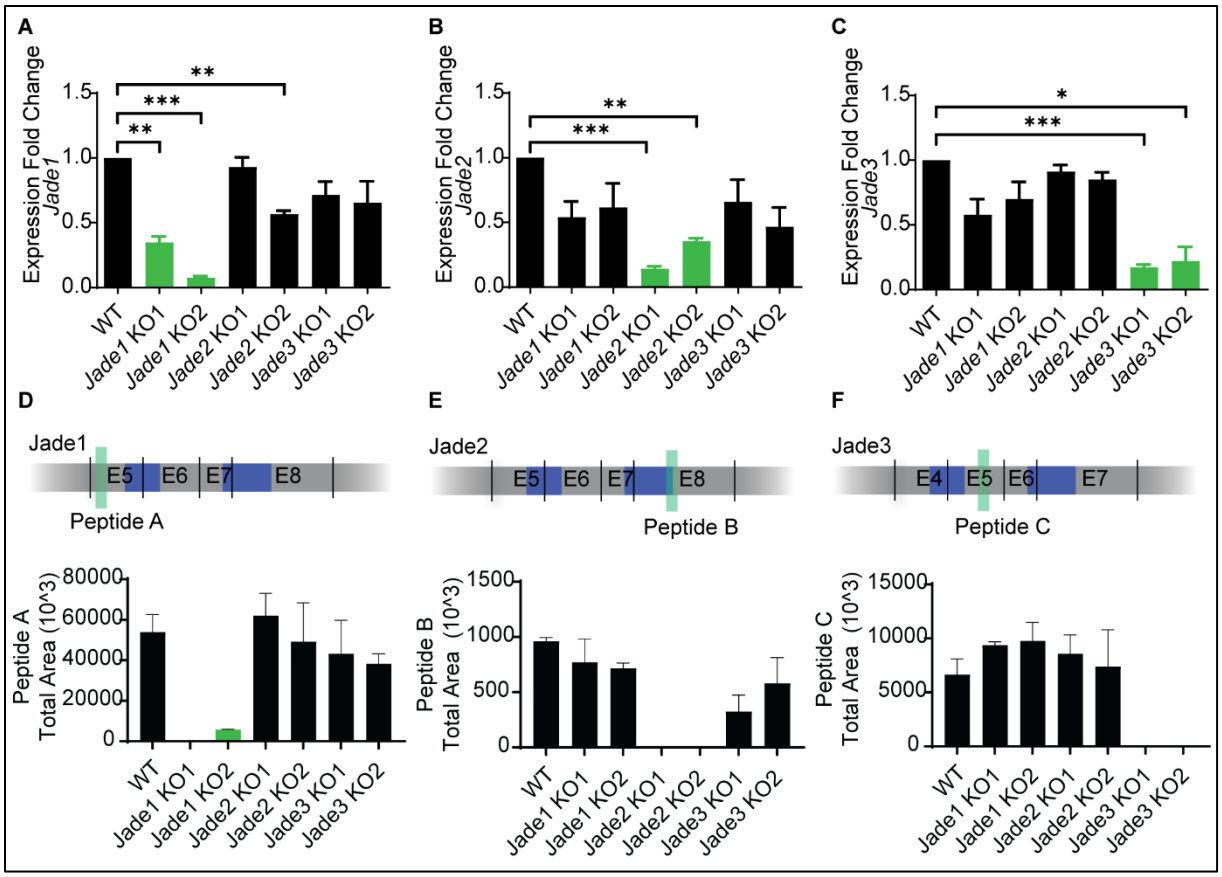

Figure 2: Deletion of one specific Jade protein does affect neither transcription nor expression of the remaining family members. (A-C) qPCR data comparing the expression fold change of each targeted gene across the different cell lines. Only the expression of the targeted gene in the respective mutant cell lines is significantly reduced, while the other Jade mRNAs are not significantly altered. (N=3, students t-test, * $p \leq 0.05$, ** $p \leq 0.01$, *** $p \leq 0.001$) **(D-F)** Parallel reaction monitoring (PRM) assay for **(D)** Jade1, **(E)** Jade2, and **(F)** Jade3 comparing the peak areas for the selected peptides across mIMCD3 WT and Jade mutant cell lines for protein quantification. The localization of peptides selected for PRM assay is depicted above the bar charts. (N=3)

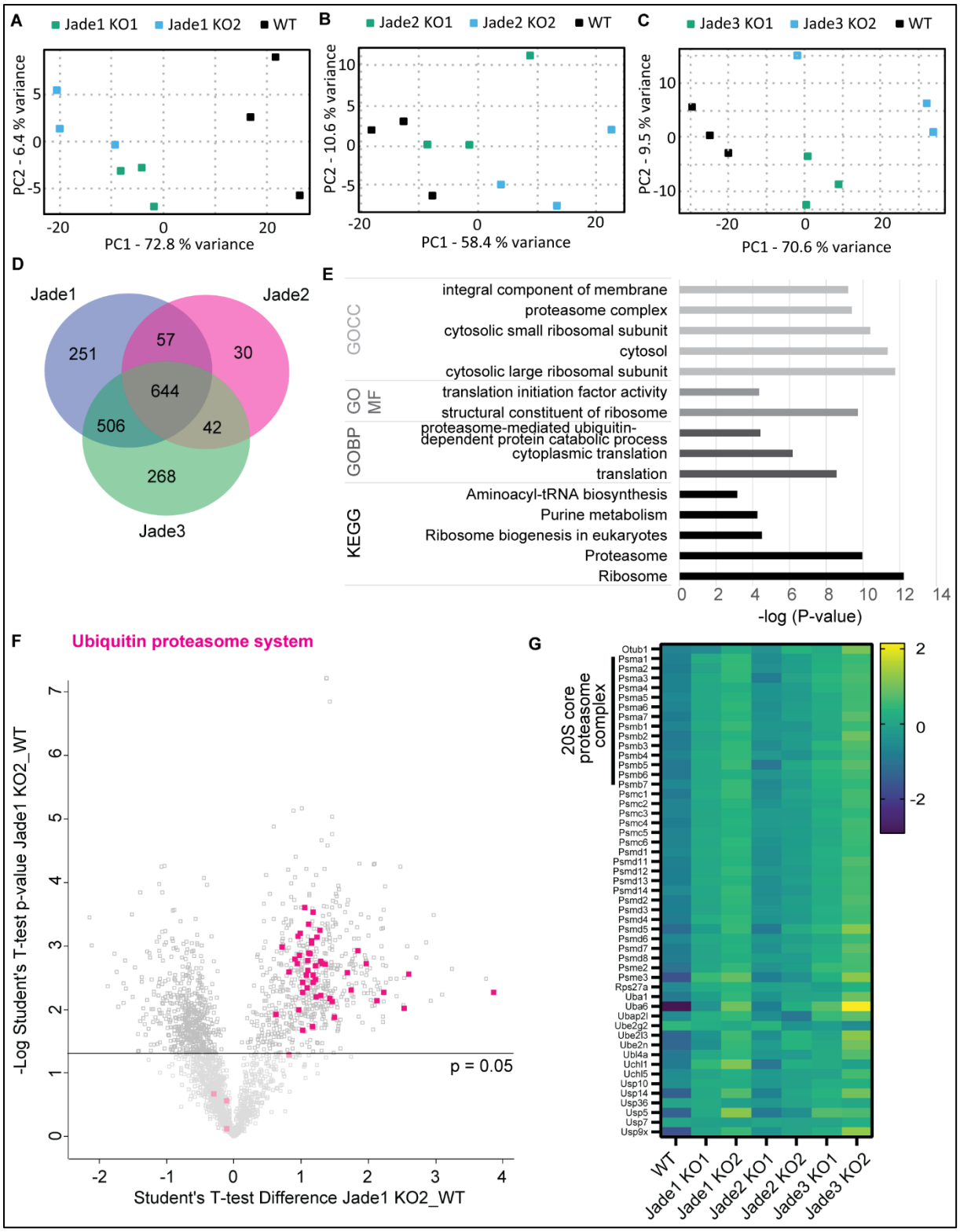

Figure 3: Proteomic analysis reveals upregulation of the proteasome in cell lines lacking either one of the Jade family members. (A-C) Principal component analysis (PCA) plot of the protein expression data of WT, Jade1 (A), Jade2 (B), and Jade3 (C) KO1 and KO2 cell lines. Depicted are the first two principal components (PC1 and PC2). The axes represent the percentages of variation explained by the principal components. The replicates of the different groups cluster together and the difference between mutant and wildtype groups explains the largest variance. (D) Venn diagram depicting the

824 overlap between significantly regulated proteins across the Jade-deficient cell lines. The Jade1 section
825 includes all proteins that are significantly regulated (p-value < 0.05) in either one or both of the Jade1-
826 deficient cell lines. The Jade2 and Jade3 sections generated in the same way. (E) GO and KEGG pathway
827 annotation based on a Fisher exact test of the 644 proteins found to be regulated in all Jade mutant
828 cell lines. (F) Representative scatter plot with the t-test differences in protein expression of the Jade1
829 KO2 mutant cells vs the wildtype cells on the x-axis and the statistical significance ($-\log_{10}$ Student's t-
830 test p-value) on the y-axis. Proteins associated with the ubiquitin proteasome system are highlighted
831 in magenta. (G) Heatmap of the proteins highlighted in (F) based on logarithmized LFQ values for all
832 Jade-deficient cell lines and the control line visualizing the upregulation of proteasome-associated
833 proteins.
834

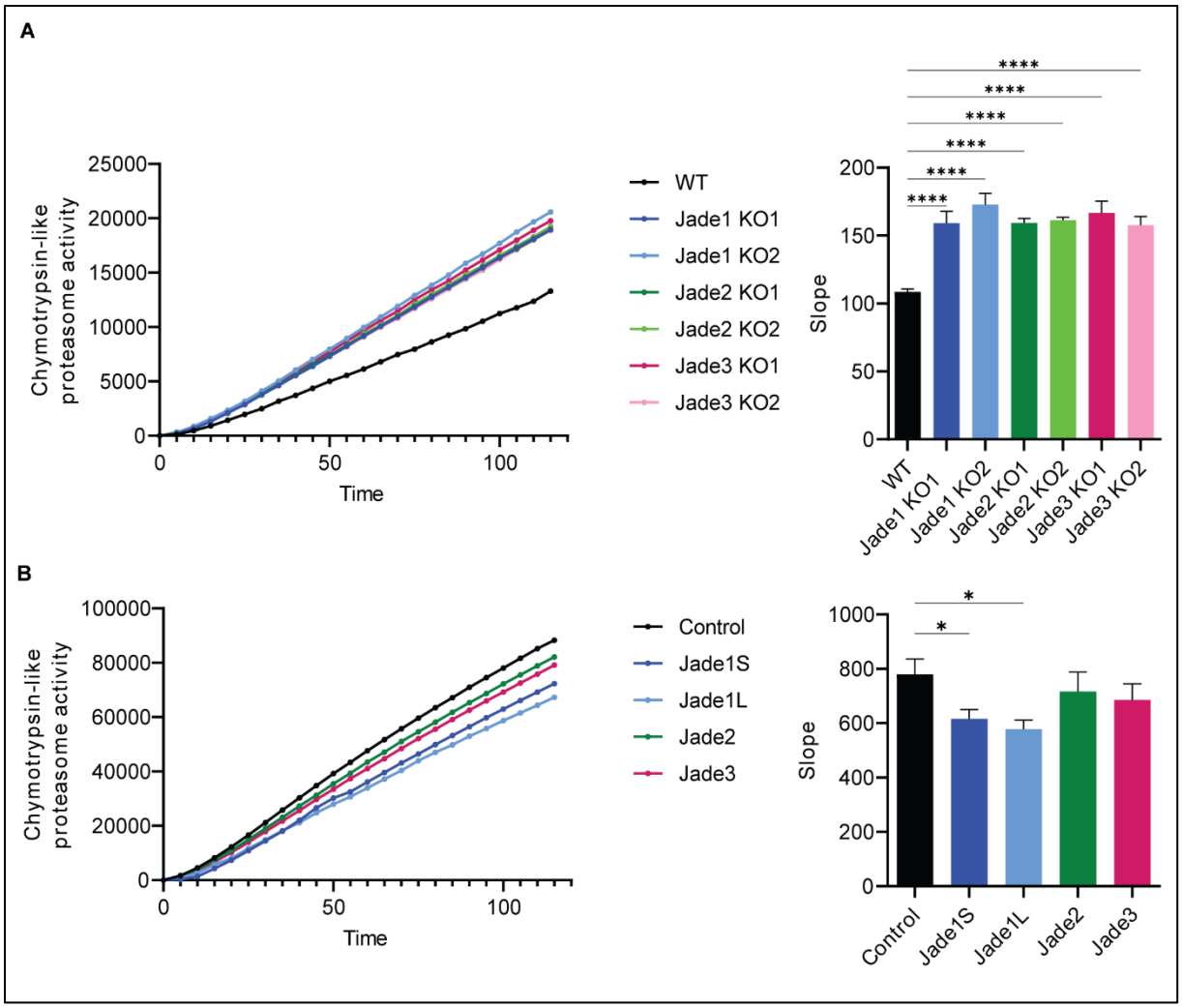

Figure 4: Increased proteasome activity observed in Jade-deficient cell lines. (A) Measurement of the proteasome activity in wildtype and Jade-deficient mIMCD3 cell lines. The proteasome activity of Jade1, Jade2, or Jade3-deficient cell lines is increased compared to the wildtype control. Quantification of the slope as readout for proteasome activity (N=3, one-way ANOVA with Dunnett's post-hoc test, ****$p \leq 0.0001$) **(B)** Measurement of the proteasome activity in HEK293T cell with either Jade1S, Jade1L, Jade2, Jade3, or Podocin (control) overexpressed. All cell lines with overexpressed Jade proteins show a decreased activity compared to the control with only Jade1S/L reaching statistical significance. Quantification of the slope as readout for proteasome activity (N=3, one-way ANOVA Dunnett's post-hoc test, * $p \leq 0.05$)

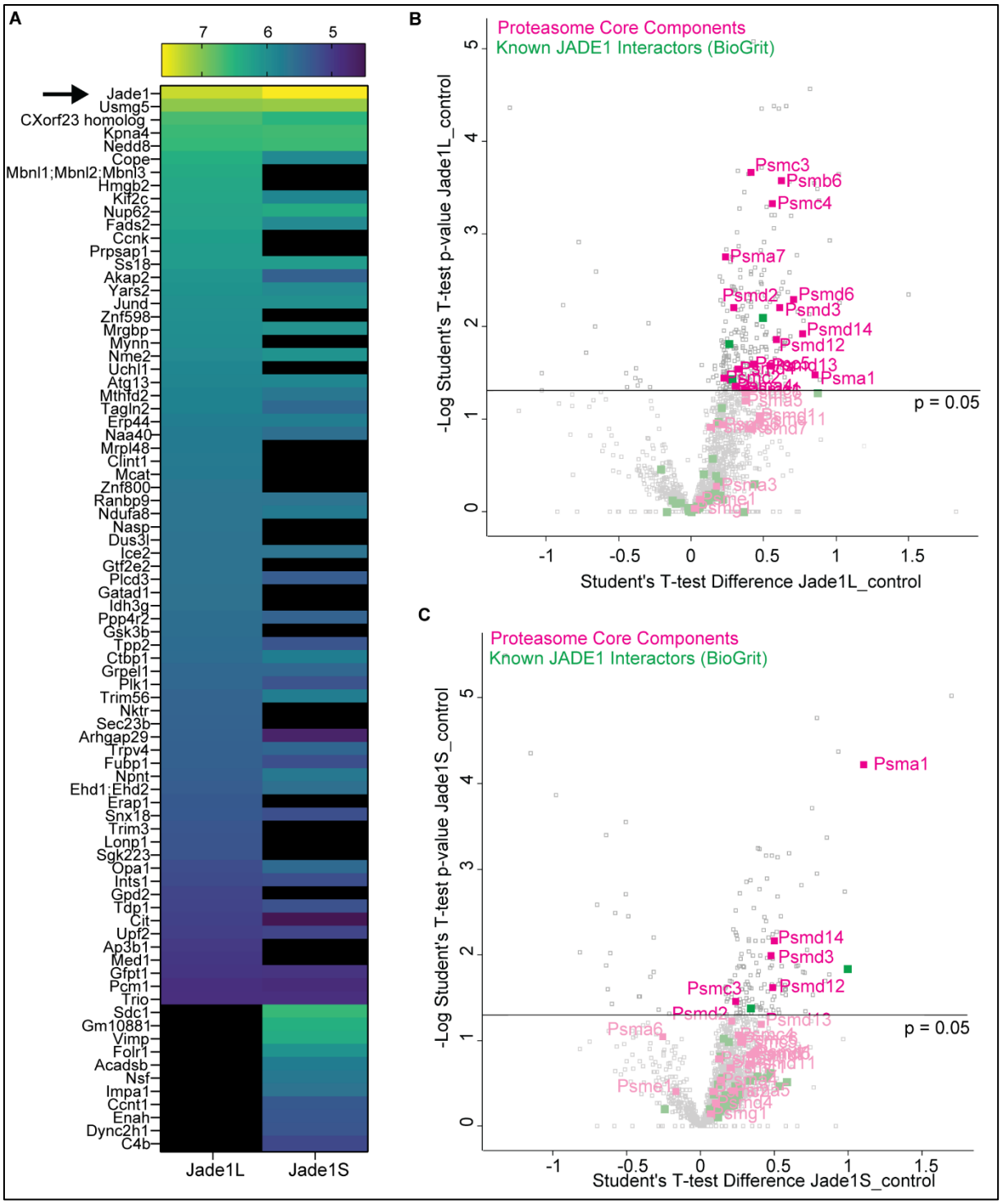

845

846 **Figure 5: Interactome analysis reveals a link between Jade1L/S proteins and proteasomal**
847 **components. (A)** Jade1 KO1 mIMCD3 cells were transiently transfected with either Flag-tagged Jade1L,
848 Jade1S, or a control plasmid. Pulldown was performed with anti-Flag (M2) sepharose beads. Heatmap
849 of average iBAQ values for proteins which were never measured in the control samples, but in either
850 all replicates for Jade1L, all replicated for Jade1S, or all replicates of both. The protein with the highest
851 iBAQ is Jade1 for both, the Jade1S and the Jade1L pulldown. **(B/C)** Quantitative analysis of the Jade1L
852 **(B)** & Jade1S **(C)** interactome. Proteins on the right side, above the p=0.05 line, are determined

853 significantly enriched. Proteasomal components are highlighted in magenta, known JADE1/Jade1
854 interactors based on known interactors annotated in BioGrid (54) in green.